Uniaxial dielectric anisotropy in $Ba_{0.5}Sr_{0.5}TiO_3$ films studied by evanescent-probe microscopy

Y.G. Wang and M. E. Reeves
The George Washington University, Washington, DC 20052

W.J. Kim, J.S. Horwitz and F.J. Rachford
Naval Research Laboratory, Washington, DC 20375
(March 30, 2001)

The dielectric permittivity, tunability ($\Delta\epsilon/\epsilon$), and loss tangent of $Ba_{1-x}Sr_xTiO_3$ (BST) films grown by pulsed-laser deposition are studied by near-field microwave microscopy. Based on theoretical simulations, a method is developed to measure the uniaxial dielectric anisotropy, $\epsilon_\perp/\epsilon_\parallel$, in BST films grown at different oxygen pressures. The measured $\epsilon_\perp/\epsilon_\parallel$ decreases with the film-growth oxygen pressure, consistent with the structural anisotropy. The films prepared at 50 mT, with $\epsilon_\perp \approx \epsilon_\parallel$, have the highest permittivity, tunability, and figure of merit.

77.84.Dy, 77.22.Ch, 77.80.Bh, 81.40.Gh

$Ba_{1-x}Sr_xTiO_3$ (BST) thin films have a high dielectric permittivity that can be tuned by a bias electric field. As a result, they have been studied extensively and are being used to develop microwave devices, such as tunable oscillators, delay lines and phase shifters.[1–5] The dielectric properties of BST films can be optimized for device operation at different temperatures. At room temperature $Ba_{0.5}Sr_{0.5}TiO_3$ films have high dielectric permittivity and tunability because their Curie temperature is just below the room temperature. To measure the microwave dielectric properties, interdigitated electrodes[1–4] and near-field scanning microwave microscopy[6,7,9,10] have been used. The former method measures mainly the in-plane dielectric properties[2] while the latter detects a combination of both the in-plane and out-of-plane components of dielectric matrix and is able to map the local variation of dielectric properties.[7] Measurements by the two methods can give different results if the sample is dielectrically anisotropic.

Anisotropy is often an essential property of dielectrics, whether arising from intrinsic[11] or extrinsic sources[2,4]. Thin films of the bulk isotropic materials can become anisotropic due to the biaxial stress[2,4] imposed by substrates and/or surface effects.[12] Considering the many applications dependent on dielectric films like BST, it is not only scientifically interesting but also practically important to develop a means to measure the dielectric anisotropy of films. Thus, in this paper we develop a method to characterize the dielectric anisotropy of a series of BST films with known structural anisotropy, based on calculations of the resonant frequency of a near-field microwave microscope as a function of dielectric anisotropy. We also measure the dielectric permittivity, tunability, and loss tangent of the BST films by near-field microwave microscopy.

The 500 nm thick BST films are grown by pulsed laser deposition onto (001) MgO single crystals using a stochiometric $Ba_{0.5}Sr_{0.5}TiO_3$ target.[1,2] The oxygen pressure in the deposition chamber varies from 10 to 500 mTorr, while the substrate temperature is maintained at 750 ^{0}C. The dielectric properties are measured using a near-field microwave microscope consisting of a quarter wavelength cavity and an HP8753D Network Analyzer.[7] An electrochemically polished tungsten tip protrudes from the central conductor of the cavity and provides close coupling to the sample under study. Thus, the dielectric constant and loss tangent can be calculated from the measured resonant frequency and quality factor, and near-field microscopy in the submicron range can be realized.[6,7]

To accurately control the placement of the sample in three dimensions, piezoelectric actuators are used for positioning. While horizontal scans are not reported in this letter, accurate vertical positioning is critical to the results presented here. The dielectric constant measurements are made by stepping the sample towards the tip in 10 nm steps until the sample just contacts the tip (areal measurements could be implemented by simply moving the sample to a new position and repeating the vertical scan). The dielectric constant is then calculated from the slope of the change in resonance frequency, df/dz.[8] In these measurements, 20 vertical scans are made for each data point. The possibility of tip damage is assessed by checking the consistency of the data over time, and by post-measurement optical imaging of the tips. In these ways we are able to rule out any significant effect due to tip blunting during the course of the experiment.

The experimental configuration is simulated by calculating the resonant-frequency shift of the cavity-tip assembly in close proximity to a dielectrically anisotropic film using perturbation theory: the small contribution of tip-sample region is assumed to be capacitively coupled to the cavity. The electric field in the tip-sample assembly is obtained by numerically solving Maxwell's equations under a static approximation considering that

the tip size and the tip-sample distance are much smaller than the wavelength (15 cm at 2 GHz). The tip is modeled as a cylinder capped by a cone with a spherical end, all held at a constant potential of 1V. For calculations with different tips, only the radius of the spherical cap, R (see inset of Fig. 1(a)), varies, while the length of the conical section and the dimensions of the cylinder remain constant. We also use a commercial software package, Maxwell 3D Field Simulator,[13] to verify our results.

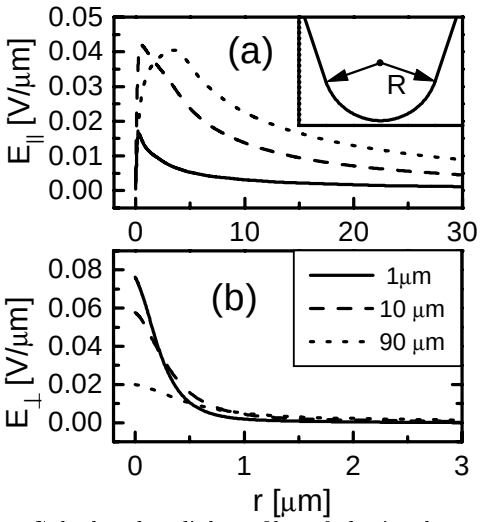

FIG. 1. Calculated radial profiles of the in-plane, $E_{\parallel}$, and out-of-plane, $E_{\perp}$, components of electric field in a film with a thickness of 0.5 μm and ϵ=300. The solid, dashed, and dotted curves are results calculated at tip radii, R, of 1, 10, and 90 μm, respectively. The substrate has an ϵ=10. The inset in (a) shows the ending part of a tip composed of a conical and a spherical section with radius R.

Our calculations reveal the interesting result that the ratio of the out-of-plane vs. in-plane component of the probe field, $E_{\perp}/E_{\parallel}$(or E_z/E_r in cylindrical coordinates), decreases with increasing tip radius. This is demonstrated in Figure 1, where we plot radial profiles of $E_{\parallel}$ and $E_{\perp}$ in the central plane of a 0.5 μm film. The curves shown in the Figure are calculated for three tips with radii, R, of 1 (solid), 10 (dashed), and 90 μm (dotted), respectively. The film and substrate have dielectric constants of 300 and 10, respectively. As expected, both the $E_{\parallel}$ and $E_{\perp}$ in the film decrease radially. However, the $E_{\perp}$ is mainly concentrated in a region with a diameter about 1 μm below the tip, while the effective area of $E_{\parallel}$ is much larger and depends more strongly on the tip size (note the difference in x-axis scales in Fig. 1 (a) and (b)). As a result, the total $E_{\perp}/E_{\parallel}$ decreases with tip radius. For example, the calculated average values of $E_{\perp}/E_{\parallel}$ are 0.4, 0.14, and 0.01 for tips with radii of 1, 10, and 90 μm, respectively. This implies that small tips detect a combination of the in-plane and out-of-plane components while large tips are mainly sensitive to the in-plane component of the dielectric matrix of the film.

The sensitivity of $E_{\perp}/E_{\parallel}$ on tip radius indicates that dielectric anisotropy, $\epsilon_{\perp}/\epsilon_{\parallel}$, can be measured by using different-sized tips. This is shown by the dependence of the calculated shifts in resonant frequency on film dielectric anisotropy for different tip radii (see Fig. 2). Considering that the total shift in resonant frequency, Δf, increases with tip size, the curves are scaled to intersect for the isotropic case. For all calculations, the average dielectric constant, $(\epsilon_{\parallel} \times 2 + \epsilon_{\perp})/3$, of the film is held fixed. It is obvious that larger tips are more sensitive to dielectric anisotropy. This can be understood from the dependence of $E_{\perp}/E_{\parallel}$ on tip size.

We experimentally demonstrate the decreasing sensitivity to $\epsilon_{\parallel}$ for sharper tips by measuring the tunability of a BST film grown in 50 mT of oxygen. 50 μm and 1 μm tips are placed in the center of a 100 μm gap between two parallel, coplanar electrodes. When an electric field of 1.5 V/μm is applied, the dielectric constant decreases by 22% and 15% respectively for the 50 μm and 1 μm tips. These results are consistent with our simulations. However, the measured tunabilities are lower than the 60% reported in Reference 1, where a higher bias field of 8 V/μm is used and where, unlike our measurements, the microwave and dc-bias electric-field vectors are parallel.

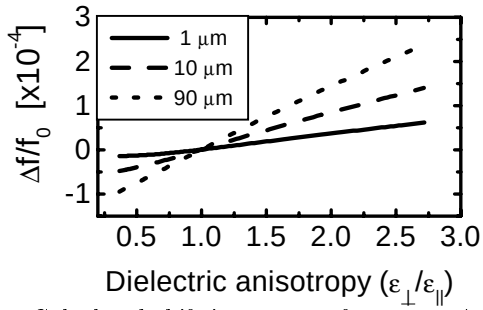

FIG. 2. Calculated shift in resonant frequency, Δf, of the cavity vs. film dielectric anisotropy and tip radius. The values of Δf are scaled to intersect when $\epsilon_{\parallel} = \epsilon_{\perp}$, and the average dielectric constant of the film, $(\epsilon_{\parallel} \times 2 + \epsilon_{\perp})/3$, is kept constant. f_0 is the resonant frequency of the cavity.

The dielectric permittivities of BST films grown at oxygen pressures of 10, 50, 350, and 500 mT are measured using a microwave microscope. Fig. 3 (a) shows the measured shifts in resonant frequency for tips with radii R identical to those used in the simulations. The values of Δf are scaled so that measurements of a bare MgO substrate using different-sized tips are coincident. With increasing tip radius, the measured Δf decreases for the films grown at 10 mT, and increases for films grown at 350 and 500 mT. For the films grown at an oxygen pressure of 50 mT, there is negligible difference between measurements with different-sized tips. The frequency shifts shown here can be converted into the dielectric anisotropy of the BST films by comparing these results with the calculations shown in Fig. 2. The comparison reveals that $\epsilon_{\perp}/\epsilon_{\parallel}$ >1 for the films grown at 10 mT, $\epsilon_{\perp}/\epsilon_{\parallel}$ <1 for the films grown at 350 and 500 mT, and $\epsilon_{\parallel}/\epsilon_{\perp}$ ≈1 for the films grown at 50 mT. The ob-

tained dielectric anisotropy agrees qualitatively with the structural anisotropy obtained by x-ray diffraction, as shown in Fig. 3 (b). Hence, the ratio of out-of-plane vs. in-plane lattice parameter, $a_\perp/a_\parallel$, and the ratio of $\epsilon_\perp/\epsilon_\parallel$ show the same dependence on film-growth oxygen pressure. To quantitatively determine the dielectric anisotropy, however, samples with known in-plane and out-of-plane dielectric permittivities are needed for calibrations.

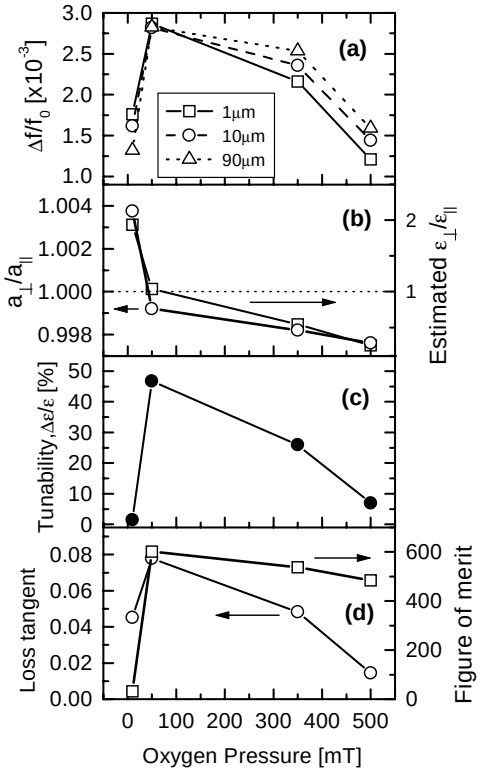

FIG. 3. The measured shifts in resonant frequency using different-sized tips (a), dielectric anisotropy and lattice parameters (b), tunability at 4 V/μm (c), and loss tangent and figure of merit (d) of $Ba_{0.5}Sr_{0.5}TiO_3$ films as functions of film-growth oxygen pressure.

The correlation between the structural and dielectric anisotropies seems to suggest a rotation of polar axis of the ferroelectric-tetragonal phase in films grown under increasing oxygen pressure. However, the films are nominally paraelectric at room temperature,[1,14] and we propose that the observed lattice deformations arise from the interplay between stress and self-ordering of oxygen vacancies. It has been known since the work of Grenier *et al.*[15] that an increase in the density of oxygen vacancies in the perovskites leads to two-dimensional planar ordering. In this picture, the oxygen vacancies cause the structure to deform, and so introduce ordering fields within the film, which results in dielectric anisotropy. This behavior is also observed as soft-mode hardening in $SrTiO_3$ films[17] and single crystals[18]. Thus, increasing the oxygen pressure during deposition reverses this tendency by reducing the density of oxygen vacancies and consequently changes the film dielectric anisotropy. On the other hand, the contributions of ferroelectric nanodomains in the films cannot be excluded because BST films show many characteristics of relaxors, namely, significant broadening of the phase transition and the coexistence of paraelectric and ferroelectric phases.[14] Notably, the same dependence of structural anisotropy on oxygen pressure is reported for $PbTiO_3$ films on MgO substrates.[16]

The tunability and loss tangent of a set of BST films have also been measured, with the results shown in Fig. 3 (c) and (d), respectively. For studying the tunability, films with interdigitated electrodes are used, and DC bias fields up to 4V/μm are applied between the fingers, with the tip placed in the center of the gap. The measurements reported in Reference 1 show the same dependence of tunability and figure of merit (Figure of merit = $(\Delta\epsilon/\epsilon)/tan\delta$) on oxygen pressure. Films prepared at 50 mT, with $\epsilon_\perp$=$\epsilon_\parallel$, have the highest tunability and figure of merit. For films deposited at 10 mT, the measured dielectric permittivity and loss tangent are markably higher than those in Reference 1, which is expected, since the latter measurement is insensitive to $\epsilon_\perp$.

It should be mentioned that the method to measure dielectric anisotropy with different-sized tips will also work at low frequency because of the static approximation used in the simulations. In some geometries, an electrode is placed below the film. Then the calculated $E_\perp/E_\parallel$ is expected to increase rather than decrease with increasing tip radius.

Acknowledgements: This work is supported by the DARPA FAME program through NRL grant N00173981G013. The authors would like to thank W. Kleemann, J.M. Byers, and J. Levy for helpful discussions.

[1] W.J. Kim. W. Chang, S.B. Qadri, J.M. Pond, S.W. Kirchoefer, D.B. Chrisey and J.S. Horwitz, Appl.Phys.Lett. **76**, 1185 (2000).

[2] W. Chang, J.S. Horwitz, A.C. Carter, J.M. Pond, S.W. Kirchoefer, C.M. Gilmore, and D.B. Chrisey, Appl. Phys. Lett. **74**, 1033 (1999), Wontae Chang, Ph.D. Thesis in Materials Science, School of Engineering and Applied Science, George Washington University, (1999).

[3] S. Zafar, R.E. Jones, P. Chu, B. White, B. Jiang, D. Taylor, P. Zurcher, and S. Gillepsie, Appl. Phys. Lett. **72**, 2820 (1998).

[4] T.M. Shaw, Z. Suo, M. Huang, E. Liniger, R.B. Laibowitz, and J.D. Baniecki, Appl.Phys.Lett. **75**, 2129 (1999).

[5] C.M. Carlson, T.V. Rivkin, P.A. Parilla, J.D. Perkins, D.S. Ginley, A.B. Kozyrev, V.N. Oshadchy, and A.S. Pavlov, Appl. Phys. Lett. **76**, 1920 (2000).

[6] C. Gao, and X.D. Xiang, Rev. Sci. Instrum. **69**, 3846 (1998); Y. Lu, T. Wei, F. Duewer, Y. Lu, N.B. Ming, P.G. Schultz, and X.D. Xiang, Science **276**, 2004 (1997).
[7] Y.G. Wang, M.E. Reeves, and F.S. Rachford, Appl. Phys. Lett. **76**, 3295 (2000).
[8] Y.G. Wang, M.E. Reeves, W. Chang, J.S. Horwitz, and W. Kim, Mat. Res. Soc. Proc. **603**, 221 (2000).
[9] D.E. Steinhauer, C.P. Vlahacos, F.C. Wellstood, S.M. Anlage, C. Canedy, R. Ramesh, A. Stanishevsky, and J. Melngailis, Appl. Phys. Lett. **75**, 3180 (1999).
[10] Y. Cho, S. Kazuta, and K. Matsuura, Appl. Phys. Lett. **75**, 2883 (1999).
[11] Y. Xu, Ferroelectric Materials and Their Applications (Elsevier Science, Amsterdam, 1991).
[12] W.L. Zhong, Y.G. Wang, and P.L. Zhang, Ferroelectrics Review 1, 131 (1998); Y.G. Wang, W.L. Zhong, and P.L. Zhang, Phys.Rev. **B 53**, 11439 (1996).
[13] Maxwell 2D and 3D field simulators, Ansoft Inc., Four Station Square Suite 660, Pittsburgh, PA 15219.
[14] C. Hubert, J. Levy, A.C. Carter, W. Chang, S.W. Kiechoefer, J.S. Horwitz, and D.B. Chrisey, Appl. Phys. Lett. 71, 3353 (1997).
[15] J.C. Grenier, J. Durier, M. Pouchard, and P. Hagenmuller, Mater. Res. Bull. **11** 1219 (1976).
[16] S.Y. Kweon, S.H. Yi, and S.K. Choi, J. Vac. Sci. Technol. A **15**, 57 (1997).
[17] A.A. Sirenko, I.A. Akimov, J.R. Fox, A.M. Clark, W. Si, X.X. Xi, Phys. Rev. Lett. 82, 4500 (1999); A.A. Sirenko, C. Bernhard, A. Golnik, A.M. Clark, J. Hao, W. Si, X.X. Xi, Nature **404** 373 (2000).
[18] J. Hemberger, P. Lunkenheimer, R. Viana, R. Böhmer, and A. Loidl, Phys. Rev. B **52**, 13159 (1995).